Received 31 July 2026; accepted 16 August 2026. Date of publication 31 August 2026; date of current version 14 October 2026.
The review of this paper was arranged by Associate Editor Farzaneh Ahmadi.
Digital Object Identifier 10.1109/OJIM.2026.3728937

Design and Validation of a Compact Radio Frequency Measurement System for Volumetric Near-Field Scans

NILS BADE, DOMINIK LANGER (Graduate Student Member, IEEE), AND ALEXANDER KOELPIN (Fellow, IEEE)

Institute of High-Frequency Technology, Hamburg University of Technology, Hamburg 21073, Germany

(CORRESPONDING AUTHOR: N. BADE (n.bade@tuhh.de)

ABSTRACT This work presents a modular near-field (NF) measurement system derived from the open-source 3-D printer project *RatRig V-Core 3.1*. Rather than requiring individual solutions for specific measurement tasks, the system at hand serves as a centralized measurement platform for a wide range of planar and volumetric measurements. It enables automated measurements in a controlled environment with a working volume of $510 \times 450 \times 910$ mm. Concepts from Cartesian 3-D printer mechanics are leveraged to achieve high positional accuracy, with positioning errors below $20\,\mu$m. The overall cost is significantly reduced compared to conventional measurement systems, using off-the-shelf components. The modular architecture allows for pairing the setup with different measurement instruments. The influence of moving cables is investigated, and amplitude and phase stability better than 0.6 dB and 5 ° at 60 GHz is maintained across the full scan volume. An exemplary NF measurement of a horn antenna in the V-band is conducted and compared to simulation, showing good agreement. The system is released as an open-source project (*AntRig-Measurement-System*) that provides mechanical design files, automation software, and instructions for assembly and use. The proposed measurement system combines a compact, portable, cost-effective, yet flexible implementation that is easy to replicate and use, and offers accuracy comparable to that of conventional solutions.

INDEX TERMS Antenna measurements, mechatronics, millimeter wave measurements, near-field (NF) radiation pattern, NF scan.

I. INTRODUCTION

NUMEROUS applications utilize electromagnetic radiation measurements in the near-field (NF) of antennas and devices under test (DUTs) [1], [2]. NF measurements have the advantage of allowing for solving both NF and far-field (FF) problems by transformation, with setups that are significantly smaller and affordable than systems for direct FF measurements. Such setups feature an actuation system that moves a probe through the desired measurement volume while the received signal is measured by connected radio frequency (RF) equipment. In the field of electromagnetic compatibility (EMC), NF measurements enable rapid error diagnostics and simple precompliance testing, and back-projection techniques are developed that correlate NF scans to FF EMC compliance limits [3], [4], [5]. In modern communication systems and remote sensing applications, NF measurements are used to validate and calibrate FF radiation patterns of new antenna designs and arrays [6], [7], [8]. Moreover, reflective NF measurements enable estimation of the radar cross section of DUTs in compact test setups [9] and allow for investigation of NF phenomena to validate new simulation approaches [10], [11]. Although the basic requirements for NF measurement systems, e.g., movement accuracy, automation, and controlled measurement environments, are very similar for all above-mentioned applications, most measurement setups focus on a subset of them rather than offering an adaptable, generic solution. This results in a wide variety of different measurement setups that can be found in current literature and industry.

From the field of antenna measurements, three well-established NF measurement procedures are planar NF (PNF), cylindrical NF (CNF), and spherical NF (SNF) scans [12]. In [13], [14], and [15], antenna measurement systems are presented that facilitate these three measurement procedures. All setups use six-axis robot arms for probe positioning and are installed in anechoic chambers. Their high

© 2026 The Authors. This work is licensed under a Creative Commons Attribution 4.0 License.
For more information, see https://creativecommons.org/licenses/by/4.0/

mechanical complexity and size drive up overall acquisition costs, and the high number of degrees-of-freedom (DOFs) increases the time and effort required for test development as more parameters must be configured.

Alternative concepts, such as the compact antenna test range (CATR), allow for simpler test configurations with less complex actuation systems. CATRs use parabolic reflectors to create FF conditions in a small test region [16] within a compact measurement setup. These systems are commercially available, e.g., the *R&S*[1] *ATS* series [17]. However, they are limited to FF measurements and involve high acquisition costs due to the required reflectors.

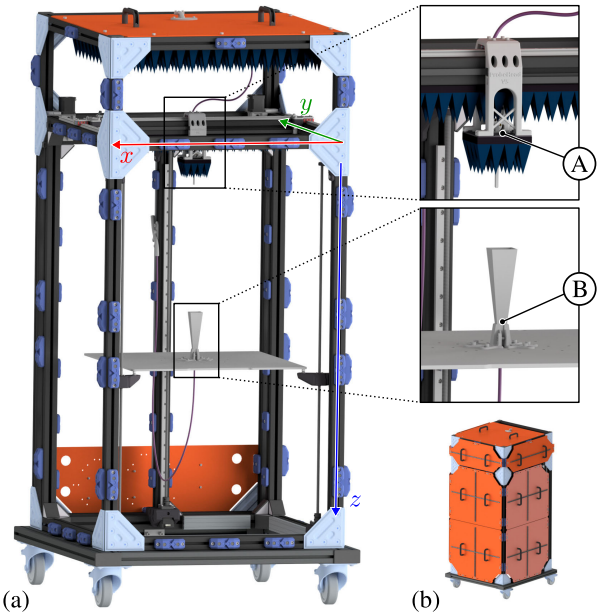
In contrast, the *Millibox* measurement systems from *Milliwave Silicon Solutions Inc.* [18] are low-cost solutions. These systems are designed to be simple, portable, and cost-effective and are meant to be deployed for testing hardware for 5G, 6G, and millimeter-wave applications. However, *Millibox* systems are also limited to FF measurements, reducing their potential fields of application.

In [19], a custom setup for volumetric and PNF measurements in the W-band is presented. The table-top setup features three linear axes and one rotary stage for the probe. Additionally, the setup can be enclosed with an absorber cover, transforming the setup into a small-sized anechoic chamber. However, the manual alignment of the z-axis to the xy plane represents a challenge during assembly that is not correctable without disassembly. Moreover, the vertically aligned xy plane and integration of RF components into moving subsystems increase inertia and mechanical stress on the setup, leading to deformation and increased positioning errors at high movement speeds.

The measurement setups in [8] and [20] accomplish three DOFs using three linear axes installed in series. Both setups are custom-built and move just the probe, while the DUT is stationary. Since in both setups the DUT is mechanically decoupled from the probe's actuation system, precise alignment of the DUT to the measurement grid of the probe is challenging. In addition, no enclosure is provided that ensures a controlled measurement environment. This reduces reproducibility of measurement results and limits the possible fields of application for the setups.

The examples show that for electromagnetic radiation and NF measurements, despite similar requirements, a wide variety of different systems have emerged. Measurement setups are either commercial, certified, and costly; therefore, access is limited, or custom-built and designed for a specific task but lacking reproducibility and a systematic error analysis of the setup itself. Today, for RF measurement tasks that do not require results from a certified setup, there is no low-cost solution available for NF scans. Instead, custom development and testing are required.

This article addresses the presented gap by designing a compact, cost-efficient measurement system for PNF and volumetric NF scans. Instead of developing custom parts and controls from scratch, sophisticated open-source projects are incorporated to benefit from past and future progress. The setup, shown in Fig. 1, features a tall-cabinet form factor, suitable even for small laboratories. The actuation system comprises a 1-D and 2-D movement system for the DUT and the probe, respectively. It achieves high positional accuracy by leveraging concepts, hardware, and software from standard Cartesian 3-D printers. This allows for a highly cost-effective solution using only readily available parts. The setup's absorber-lined enclosure facilitates controlled measurements and ensures repeatable results. Pairing with various measurement equipment and installing different probes and DUTs requires only minor adaptations, making the system applicable to a wide range of measurement tasks. The system is published open-source as *AntRig-Measurement-System* on *GitHub* [21] with detailed documentation and setup instructions.



(A) Probe antenna on the 2-D movement system
(B) DUT on the 1-D movement system

FIGURE 1. Measurement system (a) without and (b) with enclosure.

Section II introduces the general requirements for PNF and volumetric NF measurement systems. Sections III and IV present the concept and design in detail, respectively. Section V validates the system performance and presents an exemplary horn antenna measurement. Finally, Section VI concludes this article.

II. REQUIREMENTS ON NF MEASUREMENT SYSTEMS

This work focuses on PNF and volumetric NF scans. In general, for volumetric scans, the mechanical setup of the measurement system must provide at least three DOFs to position a probe relative to the DUT. The relative orientation and position of both components must be precisely known.

[1]Registered trademark.

To enable broad applicability of the system, it must allow for installation of different probes, DUTs, and combination with diverse measurement instruments for automated measurement processes. For instance, vector network analyzers (VNAs) must be pairable for antenna measurements to extract phase and amplitude information, e.g., with an open-ended rectangular waveguide (OERWG) antenna used as probe. Similarly, spectrum analyzers combined with electric or magnetic field probes must be usable to analyze present frequencies and amplitudes in EMC measurements.

Besides the paired measurement equipment, the mechanical setup itself places an upper bound to the frequency range for which the measurement system is applicable. As for higher frequencies, the field dynamics increase, and therefore, position errors lead to higher measurement errors. Consequently, the required positioning accuracy is highly dependent on the specific measurement task and its maximum operating frequency. A rule of thumb given in [12, p. 26] states that, for NF-FF transformation based on PNF scans, an, on the wavelength λ dependent, accuracy of 0.01 λ to 0.02 λ is recommended. For the presented RF measurement setup, a maximum frequency of 300 GHz is selected, resulting in a maximum positioning error of 20 μm. Since the required measurement volume is highly application-dependent, the design must allow for easy scaling to different measurement volumes without requiring significant redesign or increasing positioning errors. To achieve reproducibility of measurement results, the overall setup must ensure a controlled measurement environment, e.g., by deploying an absorptive, shielding enclosure.

Secondary goals for a generic NF measurement system are ease of use and adaptability. For this, a modular system with standardized interfaces is required. Furthermore, simple kinematics and a straightforward control architecture are favorable to make the system robust, easy to maintain, and adaptive to new measurement tasks. Finally, the system must be cost-effective, space-efficient, well-documented, and easy to replicate. Also, portability has to be considered to enable deployment in small laboratories in various locations.

III. CONCEPTUAL DESIGN

To ensure modularity and simplicity, the overall measurement system is divided into the mechanical, the measurement, and the control subsystem. Each of them features defined interfaces and can be assembled and tested independently.

The control subsystem controls the measurement process by managing the other two subsystems, as illustrated in Fig. 2. It is implemented on an external host computer, allows for configuration and monitoring of measurements, and enables display of measured data.

The measurement subsystem comprises RF measurement equipment, the DUT, the probe, and RF cables. It is remotely operated to perform RF measurements and transfer data to the control subsystem. For the remote interface, the virtual instrument software architecture (VISA) protocol is used. The RF cables are required to connect the DUT and the probe to

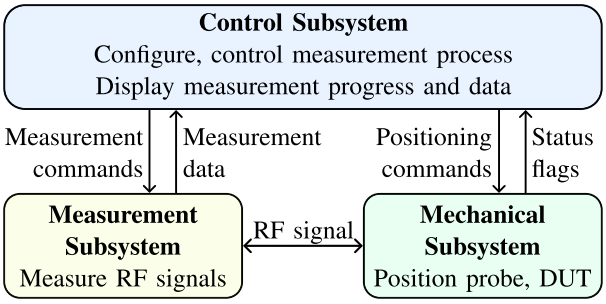


FIGURE 2. Concept sketch of the subsystems with their associated tasks.

the measurement equipment while allowing for movement within the measurement volume. The DUT, the probe, and the RF cables cannot be generalized across all applications and frequencies and must be selected per measurement task. These components define mechanical requirements for mounting and connectivity within the mechanical setup.

The mechanical subsystem positions the probe relative to the DUT within the measurement volume. Generic mountings allow for installation of various DUTs and probes, while flexible RF cables are rigidly mounted to provide connection points on the outside of the setup. The actuation is positioned close and parallel to the measurement volume to maximize space efficiency. Easy mobility of the setup is enabled by installation on a rolling base. A detachable enclosure ensures a controlled measurement environment while allowing for quick access to all components of the setup. The subsystem features an Ethernet interface for external control by the control subsystem.

IV. SYSTEM DESIGN

At the core of the designed measurement system lies the mechanical subsystem. It achieves the required three DOFs with simple kinematics by splitting the actuation into two subsystems: a 2-D movement system and a 1-D movement system aligned orthogonally. The probe is assigned to the 2-D movement system, while the DUT stays centered inside the measurement volume, mounted to the 1-D movement system.

A proven kinematic concept that aligns with these requirements is the *CoreXY* concept, widely used in Cartesian fused deposition modeling (FDM) 3-D printers. Such printers employ a belt-driven 2-D movement system for the print head [Fig. 3(b)] and a lead screw-driven 1-D movement system for the print bed [Fig. 3(c)]. For actuation, stepper motors are mounted near the working volume, thereby achieving high compactness for the overall setup. The concept enables the use of standard, high-quality parts at low cost, sourced from the large 3-D printer market. Additionally, by building on established open-source 3-D printer projects, existing design data and mature control software can be reused to maximize the reliability and accuracy of the setup.

The presented system is inspired by the open-source 3-D printer project *RatRig V-Core 3.1* [22], shown in Fig. 3(a).

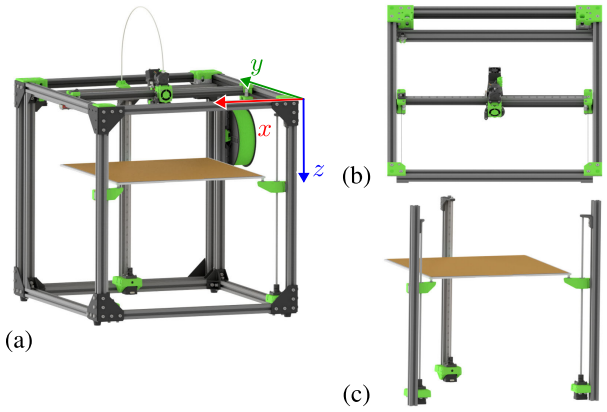


FIGURE 3. (a) 3-D model of the *RatRig V-Core 3.1* printer [22]. (b) 500 mm × 500 mm xy-movement system. (c) 500 mm z-movement system.

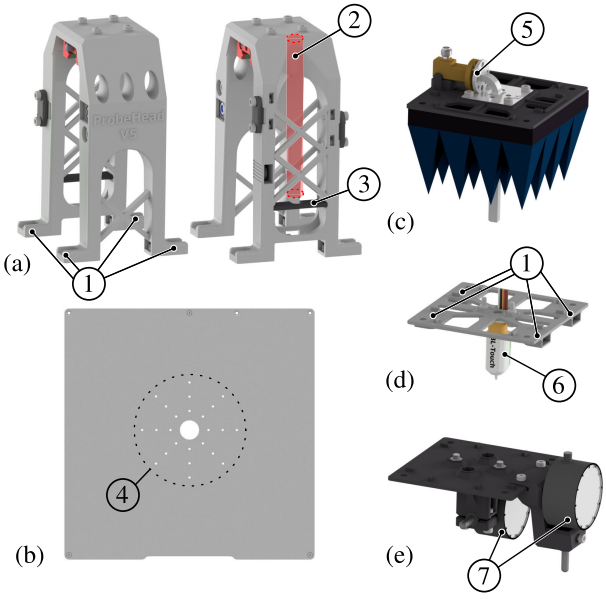
The *RatRig* employs the aforementioned *CoreXY* concept and provides a working volume of 500 × 500 × 500 mm. The low-level control for the printer is provided by the open-source project *Klipper* [23]. For interfacing, *Octoprint* [24] is used, which offers a network application programming interface (API) for custom remote control. The following Sections IV-A and IV-B describe the development of the NF measurement system with References to the *RatRig* printer design. The intended use case for the system implementation presented is PNF scanning of antennas in the V-band. Section IV-A focuses on the mechanical setup. Section IV-B presents the implementation of the control subsystem and automation. Excluding any measurement equipment, specific probe or RF cables, the overall cost for the presented measurement system is below 3500 EUR.

A. ADAPTATION OF THE 3-D PRINTER

The chosen kinematics allow for arbitrary scaling in xy-directions and z-direction to achive different measurement volumes. For the presented measurement system, a measurement volume of 510 ×450 ×910 mm is selected. Compared to the original printer, the setup is rescaled in the z-direction, and additional height is enclosed above the print head to allow for placement of absorbers and cable movement during measurement.

The original aluminum frame profiles are replaced by 39.5 % lighter wood-composite profiles from *item Industrietechnik GmbH* [25], which simplify the handling and transport of the setup. Redesigned and reselected connectors in the frame structure simplify accurate assembly and increase the frame's stiffness by providing longer lever arms, additional attachment points, and self-centring screws.

The generic fixtures for the probe and the DUT are provided at the original print head and print bed positions. The print bed is modified, renamed as "base plate" [Fig. 4(b)], and features a hole in the center ④, meant to be used as a cable feed-through in case of antenna measurements and positioning reference for arbitrary DUTs. Multiple threaded



① Magnet, screw connections
② Cable channel
③ Fixing insert
④ Generic screw mount and cable feed-through
⑤ Waveguide probe and coaxial adapter
⑥ BL-Touch sensor
⑦ Dial gauges

FIGURE 4. (a) Probe head. (b) Base plate. (c) OERWG probe module. (d) BL-Touch sensor module for z-leveling. (e) Dial gauge module for position error measurements.

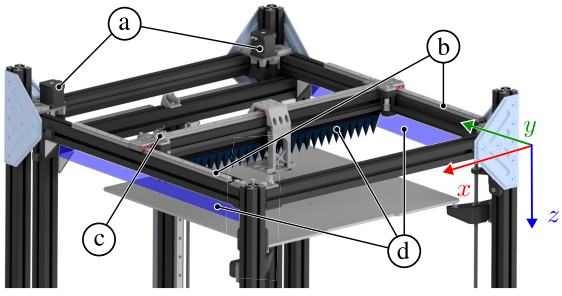


FIGURE 5. Modified xy-actuation system for the measurement setup. ⓐ Motors. ⓑ Linear rails. ⓒ X-limit switch. ⓓ Absorbers.

holes around the center allow for installation of various DUT mountings.

The original print head is replaced by the "probe head," shown in Fig. 4(a). It relocates the x-limit switch to the left end of the x-gantry (Fig. 5 ⓒ) to minimize required parts and wiring inside the measurement volume. A cable channel ② for the coaxial cable leading to the probe is provided at the back. The lower end of the channel features a fixing insert ③ to secure the screwed connection between the RF cable and the waveguide adapter ⑤ to prevent scraping and loosening during movement. Four screw connections and integrated magnets ① at the bottom of the probe head allow for installation of custom modules. One such module is shown in Fig. 4(c), which is the OERWG probe, used for

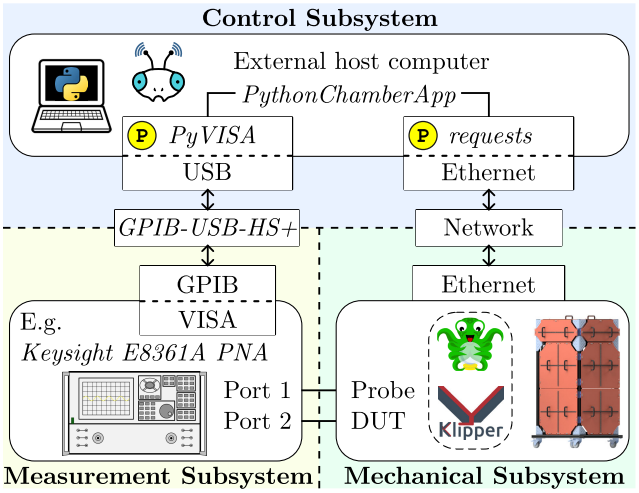


FIGURE 6. Subsystems of the measurement system with their interfaces.

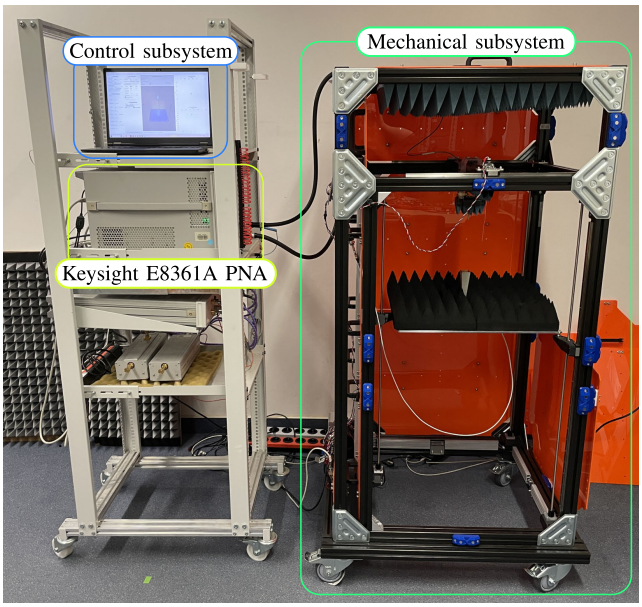


FIGURE 7. Photograph of the implemented measurement system tailored to PNF scans of antennas in the V-band.

the measurements in Section V-D. Another example is the dial-gauge module [Fig. 4(e)], used to validate the setup's movement accuracy in Section V-A.

To reduce reflections inside the measurement setup, the setup must allow for absorber installation on all parts visible from the DUT position. Thus, the *xy*-actuation is rearranged as shown in Fig. 5. The probe head provides additional space beneath the *x*-gantry to attach absorbers without colliding with the probe module. The linear rails of the *x*-gantry ⓑ are mounted on top of the frame structure, rather than underneath, to enable absorber placement ⓓ on the frame.

Finally, to isolate the measurement volume from the environment and reduce reflections at the setup's boundaries, a custom enclosure is designed. It consists of 13 acrylic glass panels with magnetic connectors for quick attachment and removal. The presented setup provides 125 mm clearance to the measurement volume, accommodating 120 mm pyramidal absorbers. However, this clearance is easily adaptable for different absorber sizes with rescaled frame-connectors. The enclosure includes fixed cable lead-throughs at the top and rear for convenient routing of the RF cables and quick connection of external equipment. Ultimately, the custom enclosure enables a simple transition between an open configuration for maintenance and setup [Fig. 1(a)] and a compact anechoic chamber for measurements [Fig. 1(b)].

The setup's firmware, composed of *Klipper* and *Octoprint*, is retained, with minor modifications to accommodate the new setup dimensions and limit switches.

B. AUTOMATION OF THE MEASUREMENT PROCESS

The control subsystem facilitates the automated measurement process. It is implemented as a custom Python application in an object-oriented fashion to ensure modularity and maintainability. The complete source code, alongside instructions for the GUI, is available in the *AntRig GitHub* repository [21]. The interface to the mechanical subsystem is provided via the *Octoprint* REST API. The interface to the measurement subsystem depends on the specific measurement equipment used. Therefore, it is implemented individually in a separate interface class. In the presented setup, an exemplary VNA, namely the *Keysight E8361A PNA*, is considered, which performs two-port S-parameter measurements between the DUT and the probe, providing amplitude and phase information. The VNA is remotely controlled via its general-purpose instrument bus (GPIB) interface and connected to the host computer via USB. An overview of the interface structure is given in Fig. 6.

Currently, the measurement system supports automated stepped scans within a cuboid measurement volume without requiring additional position sensors.

V. MEASUREMENT SYSTEM VALIDATION

In this section, the assembled measurement system is validated regarding the mechanical and electrical performance. The overall setup is shown in Fig. 7. Section V-A investigates the orientation and positioning accuracy of the probe relative to the DUT. The influence of the amplitude and phase instability of the moving RF cables is investigated in Section V-C. Finally, Section V-D presents an exemplary PNF scan of a horn antenna at 60 GHz and compares it to simulation results.

For each study, the base plate is aligned parallel to the *xy* plane of the probe head using *Klipper*'s *Z_TILT_ADJUST* procedure with the BL-Touch sensor ⑥ module [Fig. 4(d)] mounted on the probe head [Fig. 4(a)].

A. POSITIONING ACCURACY

The probe's positioning accuracy and alignment relative to the DUT are critical for accurate spatial mapping of measurement data. In the following, the positioning errors are

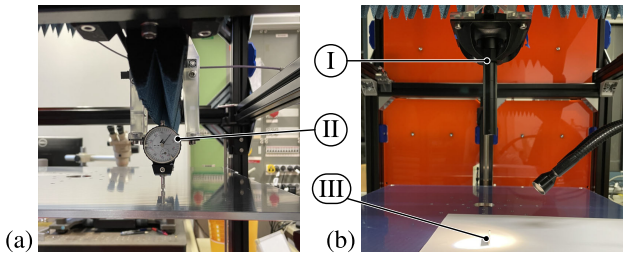


FIGURE 8. (a) Setup to validate horizontal alignment and z-step size. (b) Measurement setup to check xy-movement accuracy. (I) Telecentric camera. (II) Dial gauge. (III) Measuring gauge on base plate.

categorized as constant offset errors and relative movement errors.

Constant offset errors are introduced by the limit switches, which serve as a reference for the absolute probe position. First, because their relative position to the measurement volume depends on the assembly. Second, since the trigger points of such switches are not precisely defined, which directly affects the probe's absolute position.

Relative movement errors occur during operation and arise from imprecise movement distances and nonorthogonal movement axes. To validate the accuracy of the relative movement distance in xyz-directions, a dial gauge [Fig. 8(a)] and a telecentric camera setup [Fig. 8(b)] are used. The dial gauge setup allows for measurements in horizontal and vertical directions, as shown in Fig. 4(e). For xy-directions, measuring gauges placed on the base plate (III) are tracked over 14 steps using a telecentric camera (I) (*UI-1640LE-C-HQ*, *IDS Imaging Development Systems GmbH*) with 4 μm/ pixel resolution. The traveled distance is measured in pixels across multiple pictures of the measurement gauge and converted to micrometers. The average positioning error is -12 μm $\pm$ 4.5 μm in x-direction and -6 $\pm$ 3.9 μm in y-direction. This is close to the theoretical minimum step size of 4.42 μm/ step, based on the pulleys, the belt, and the microstep configuration of the motors. For z-direction, a dial gauge (II) is mounted vertically on the probe head. Successive steps of the base plate reveal a systematic error of 20 μm whenever the movement direction reverses. This is likely due to backlash in the lead screw decouplers and can be overcome by approaching all target positions from the same direction. Without direction changes, the z-movement error is below the 10-μm resolution of the dial gauge. This aligns with the theoretical minimum step size of 0.625 μm/ step based on the lead screws and the motor configuration used.

To validate the orthogonality of the x- and y-movement axes, an orthogonal reference angle is placed on the base plate, and its edges are probed along two sides using the dial gauge (II) horizontally mounted. The test is repeated three times at different plate positions. From the measured distance, the relative angles between the movement axes and the reference angle edges are calculated. These measurements yield an angular error of $+0.168\,^\circ \pm 0.057\,^\circ$ for the xy-movement axes. However, this error depends on the manual alignment of the x-gantry and does not represent an inherent setup limitation. By repetitive alignment procedures, it can be reduced further.

To ensure correct angular alignment of the probe to the DUT, the base plate must be parallel to the xy plane of the setup. For validation, the vertical dial gauge (II) [Fig. 8(a)] is moved across the base plate over 400 mm in x- and y-directions. The measured distance changes yield alignment errors of less than 0.018° around the x-axis and less than 0.005° around the y-axis.

B. IMPAIRMENTS BY CABLE MOVEMENT

For NF measurements, flexible connections to the probe and the DUT are required that allow for sufficient movement without affecting the magnitude and the phase of the signal. In the presented setup, two *4F multipurpose* coaxial cables from *GORE* [26] are used. They are rigidly mounted to the mechanical setup and facilitate the connection of measurement equipment located next to it. However, such flexible cables introduce amplitude and phase instabilities, as their bending and twisting angles change [27].

To connect the probe and the horn antenna, the presented setup features two WR-15 waveguide adapters at the respective locations. To quantify the impairment of the moving cables, reflect calibration standards are mounted to the adapters, and the input reflection coefficient S_{11} and output reflection coefficient S_{22} are measured with the VNA at different positions. Changes in amplitude and phase can be attributed to the moving cables, as they are the only part of the signal path that changes throughout the measurement.

Fig. 9 shows the variations caused by the probe's coaxial cable $S_{\text{Cable}} = (S_{11})^{1/2}$, referenced to the position with maximum amplitude. Each position is measured four times by moving through the measurement grid four times in a row. Fig. 9(a) and (c) shows that the average amplitude deviates less than 0.44 dB, and the phase less than 3.1 $^\circ$ across the entire xy plane. At the same time, the value at each individual position deviates significantly less over multiple measurements, as shown in Fig. 9(b) and (d).

The systematic pattern and high repeatability of the amplitude and phase deviations enable conventional VNA calibration procedures, e.g., the short-open-load-reciprocal (SOLR) calibration method [28]. Calibration measurements can be done on a coarse grid, and the estimated correction values can be interpolated for the positions in between because of the continuous error pattern. Consequently, a complete calibration can be accomplished without addressing each position of the measurement grid individually.

The DUT's coaxial cable shows a similar repeatable behavior that allows for calibration. Over the movement range 20 mm $< z <$ 870 mm, the amplitude and phase variation are less than 0.13 dB and 1.8 $^\circ$, respectively. Consequently, in case of volumetric measurements, the same calibration

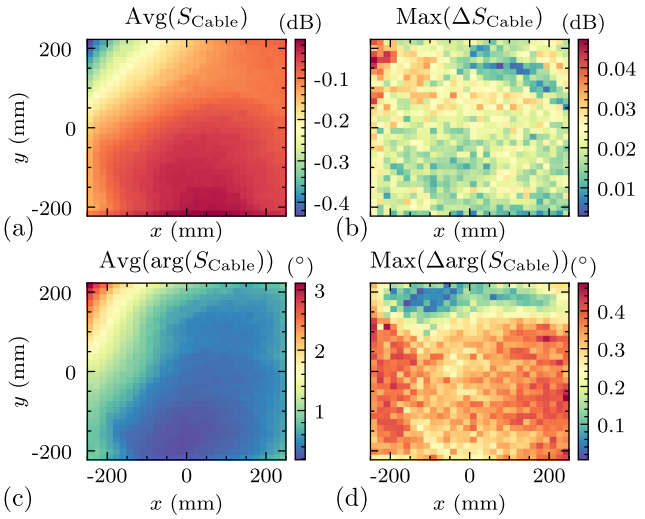


FIGURE 9. Reflect measurement over the whole xy plane with each position measured four times. (a) Normalized transmission coefficient. (b) Maximum absolute difference of forward transmission coefficient in each position. (c) Average phase. (d) Maximum absolute phase difference in each position.

procedure can be used for correction of both coaxial cables. The investigations presented in [11] and [29] are based on such calibrated measurements and prove the validity of the approach. However, Section V-D reviews the raw measurement results without any calibration applied.

C. EXEMPLARY HORN ANTENNA MEASUREMENT

As exemplary measurement, a PNF scan of a 60-GHz horn antenna with 24.8-dBi gain is performed at 200-mm distance. For probing, the OERWG probe module, shown in Fig. 4(c), is used. Because of the horn's highly directive pattern, most of the radiated power is directed toward the probe, the x-gantry, and the top panel. Consequently, in regard to internal reflections, these parts are most critical, while the side panels of the enclosure and the frame contribute less. This allows for fewer absorber installations compared to less directive DUTs, without affecting the measurement results significantly.

This assumption is validated by performing the measurement with the setup in two configurations, with and without absorbers installed. The measurements are compared to simulation results from the models shown in Fig. 10, set up in *CST Microwave Studio*. The first model, shown in Fig. 10(a), includes the DUT in free space and computes the radiated power density over a plane that is 200 mm apart from the DUT. The second model, shown in Fig. 10(b), includes simplified models of the base plate, x-gantry, and top panel positioned as in the real setup when measuring at 200-mm distance. Material losses are neglected in both models. The DUT and the base plate are modeled as perfect electric conductor (PEC). The top enclosure and the x-gantry are modeled as dielectric with a relative permittivity of 2.9 and 3.3, respectively.

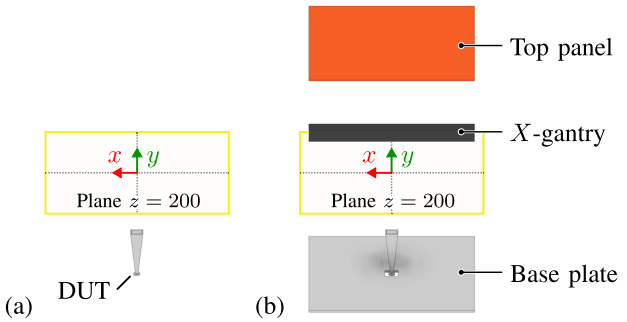


FIGURE 10. Simulation models to analyze reflections in (a) free space and (b) with the most critical reflecting parts.

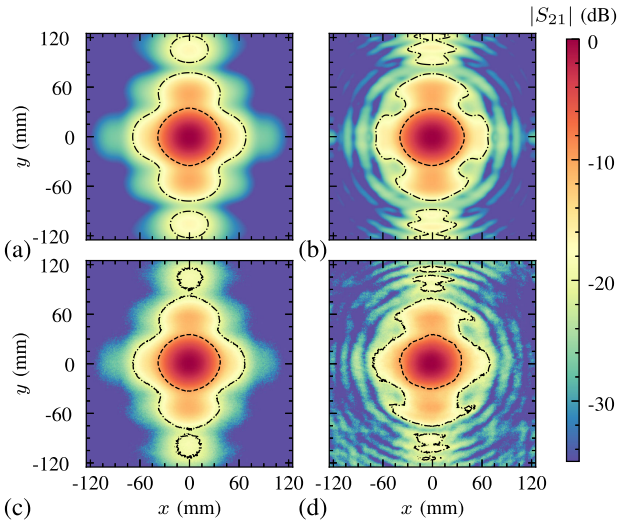


FIGURE 11. Normalized power density distribution. (a) and (b) Simulation results for the configurations in Fig. 10(a) and (b). Measurement results (c) with and (d) without absorbers installed. Contour lines at −10 dB (- · -) and −20 dB (- -) levels.

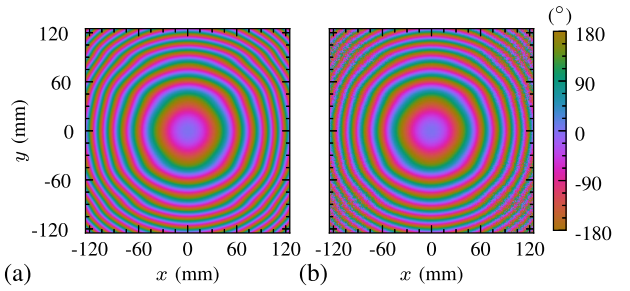


FIGURE 12. Phase distribution extracted from (a) simulation [Fig. 10(a)] and (b) measured with absorbers installed.

Fig. 11 compares simulated [(a) and (b)] and measured [(c) and (d)] power density distributions at 200-mm distance from the DUT for both configurations. A square scanning area of $|x| < 125$ mm and $|y| < 125$ mm in the xy plane is chosen to cover the main lobe and the first two side lobes of the horn antenna. The normalized power density

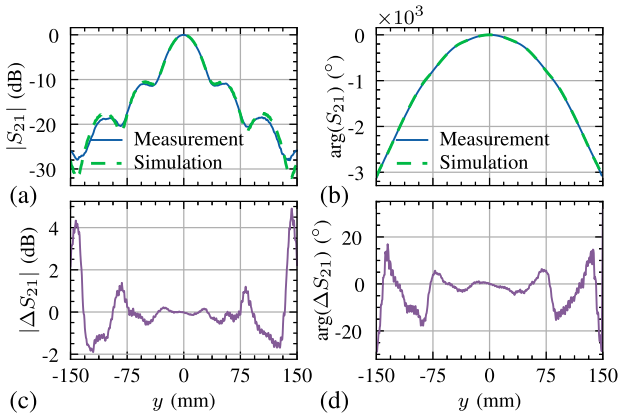


FIGURE 13. Comparison of simulated and measured results along the y-axis at 200-mm distance from the DUT. (a) Normalized power density distribution. (b) Normalized, unwrapped phase values. (c) and (d) Difference between simulation and measurement.

$P_{\text{density}}(x, y) = 20\log(|S_{21}(x, y)|/|S_{21,max}|)$ follows from the forward transmission coefficient $S_{21}(x, y)$. In Fig. 11(b), the circular pattern around the center stands out and differs from the results in Fig. 11(a). Multiple reflections between the top panel, x-gantry, and base plate are causing a standing wave pattern inside the measurement volume, which distorts the power density distribution of the free-space scenario. Fig. 11(c) and (d) presents results from two measurements using a 1-mm step size on a rectangular grid. In Fig. 11(d), the setup has no absorbers installed, while in Fig. 11(c), absorbers are placed on the top panel, x-gantry, probe head, and base plate, as shown in Fig. 7. Comparing the plots in Fig. 11(b) and (d), the similarity of the circular error pattern stands out. By installing absorbers, reflections are significantly suppressed, resulting in good agreement between the measurement results [Fig. 11(c)] and the free-space simulation [Fig. 11(a)]. This is further highlighted by the contour lines in Fig. 11. The phase measurement also aligns very well with the simulation reference, as shown in Fig. 12.

In the following, the residual measurement error of the absorber-lined setup is quantified. Thereby, the influence of the chosen OERWG probe is excluded, as the probe is not considered as part of the generic measurement system itself. For this, a free-space simulation model is set up, in which the OERWG probe, modeled as PEC, is moved to the same relative positions as in the real measurement. Then, for each position, the S_{21} parameter between the DUT and the probe is computed and extracted.

Fig. 13(a) and (b) shows the normalized power density and unwrapped phase values along the y-axis at 200-mm distance from the DUT for both simulation and measurement. Fig. 13(c) and (d) evaluates the amplitude and phase error by $\Delta S_{21} = S_{21,\text{meas}}/S_{21,\text{sim}}$. Measurement and simulation results agree very well, with less than 0.6 dB deviation in power density and below 5.6 ° phase deviation over $|y| < 75$ mm. Further away from the center, the deviations increase, showing an axis-symmetric behavior. The symmetric property suggests that residual reflections within the measurement setup remain the dominant source of error, similar to the observed errors without absorbers. However, this effect can be reduced by further optimization of the absorbers.

VI. CONCLUSION

This work presents an adaptable RF measurement system for volumetric and planar NF measurements. To fill the gap between expensive commercial solutions and low-cost but unreplicable custom setups, a modular, automated measurement system inspired by proven concepts from 3-D printing is designed. Generic interfaces allow for pairing the setup with arbitrary measurement equipment, and custom fixtures enable installation of different probes and DUTs for different measurement tasks. Positing errors of the setup are below 20 μm, allowing broad use in EMC and millimeter-wave applications with a measurement volume up to 510 × 450 × 910 mm. A controlled measurement environment is created by an absorber-lined enclosure that effectively suppresses internal reflections while maintaining a compact form factor for the overall setup. The system is validated regarding errors introduced by cable transmissions and internal reflections, and an exemplary PNF measurement of a 60-GHz horn antenna shows excellent agreement with simulation.

The designed measurement system is released as an open-source project on *GitHub* [21]. The *AntRig* project provides a detailed 3-D model, a setup guide for the system, and the source code to run the Python application that automates the measurement process.

REFERENCES

[1] A. Yaghjian, "An overview of near-field antenna measurements," *IEEE Trans. Antenn. Propag.*, vol. AP-34, no. 1, pp. 30–45, Jan. 1986.

[2] E.-X. Liu, W.-J. Zhao, B. Wang, S. Gao, and X.-C. Wei, "Near-field scanning and its EMC applications," in *Proc. IEEE Int. Symp. Electromagn. Compat. Signal/Power Integrity (EMCSI)*, Washington, DC, USA, Aug. 2017, pp. 327–332.

[3] D. Baudry, C. Arcambal, A. Louis, B. Mazari, and P. Eudeline, "Applications of the near-field techniques in EMC investigations," *IEEE Trans. Electromagn. Compat.*, vol. 49, no. 3, pp. 485–493, Aug. 2007.

[4] J.-R. Regue, M. Ribo, J.-M. Garrell, and A. Martin, "A genetic algorithm based method for source identification and far-field radiated emissions prediction from near-field measurements for PCB characterization," *IEEE Trans. Electromagn. Compat.*, vol. 43, no. 4, pp. 520–530, Nov. 2001.

[5] H. Weng, D. G. Beetner, and R. E. DuBroff, "Prediction of radiated emissions using near-field measurements," *IEEE Trans. Electromagn. Compat.*, vol. 53, no. 4, pp. 891–899, Nov. 2011.

[6] D.-H. Lee et al., "An S-band-receiving phased-array antenna with a phase-deviation-minimized calibration method for LEO satellite ground station applications," *Electronics*, vol. 11, no. 23, p. 3847, Nov. 2022.

[7] M. A. Salas-Natera, R. M. Rodriguez-Osorio, and L. De Haro, "Procedure for measurement, characterization, and calibration of active antenna arrays," *IEEE Trans. Instrum. Meas.*, vol. 62, no. 2, pp. 377–391, Feb. 2013.

[8] H. Gao, F. Zhang, M. Li, G. F. Pedersen, and W. Fan, "Development and validation of testing system for automated millimeter-wave phased array multibeam near-field measurement," *IEEE Trans. Instrum. Meas.*, vol. 72, pp. 1–14, 2023.

[9] Y.-X. Zhang, Y.-C. Jiao, M.-D. Zhu, and Y. Zhang, "Wideband near-field RCS measurement techniques with improved far-field RCS prediction accuracies," *IEEE Trans. Instrum. Meas.*, vol. 72, pp. 1–4, 2023.

[10] B. Tegowski, D. Langer, M. Wenzel, N. C. Albrecht, and A. Koelpin, "Near-field scattering phenomena in monostatic radar applications derived from physical optics," *IEEE Trans. Antennas Propag.*, vol. 73, no. 2, pp. 1084–1094, Feb. 2025.

[11] B. Tegowski, D. Langer, N. C. Albrecht, and A. Koelpin, "Fast determination of the monostatic radar channel in the near-field of electrically large targets," in *Proc. 55th Eur. Microw. Conf. (EuMC)*, Sep. 2025, pp. 610–613.

[12] IEEE Recommended Practice for Near-Field Antenna Measurements, IEEE Standard 1720-2012, 2012.

[13] D. M. Lewis, J. Bommer, G. E. Hindman, and S. F. Gregson, "Traditional to modern antenna test environments: The impact of robotics and computational electromagnetic simulation on modern antenna measurements," in *Proc. 15th Eur. Conf. Antennas Propag. (EuCAP)*, Dsseldorf, Germany, Mar. 2021, pp. 1–5.

[14] L. Boehm, F. Boegelsack, M. Hitzler, and C. Waldschmidt, "The challenges of measuring integrated antennas at millimeter-wave frequencies [measurements corner]," *IEEE Antennas Propag. Mag.*, vol. 59, no. 4, pp. 84–92, Aug. 2017.

[15] J. Zheng, X. Chen, and Y. Huang, "An effective antenna pattern reconstruction method for planar near-field measurement system," *IEEE Trans. Instrum. Meas.*, vol. 71, pp. 1–12, 2022.

[16] C. Parini, S. Gregson, J. McCormick, and D. J. Van Rensburg, *Theory and Practice of Modern Antenna Range Measurements*. Edison, NJ, USA: IET, Oct. 2014, pp. 93–210.

[17] Rohde & Schwarz GmbH & Co. KG *Antenna Test Systems and OTA Chambers*. Accessed: Nov. 13, 2025. [Online]. Available: https://www.rohde-schwarz.com/de/produkte/messtechnik/antennenmesstechnik-und-ota-kammern103249.html

[18] Milliwave Silicon Solutions Inc. *Millibox Antenna Test Systems*. Accessed: Oct. 1, 2025. [Online]. Available: https://millibox.org/

[19] G. F. Hamberger et al., "Setup and characterization of a volumetric W-band near-field antenna measurement system," *IEEE Trans. Antenn. Propag.*, vol. 66, no. 10, pp. 5498–5510, Oct. 2018.

[20] Y. Zhao et al., "Measurement of near-field electromagnetic emissions and characterization based on equivalent dipole model in time-domain," *IEEE Trans. Electromagn. Compat.*, vol. 62, no. 4, pp. 1237–1246, Aug. 2020.

[21] N. Bade. *AntRig-Measurement-System. Open-Source Repository*. Accessed: Oct. 5, 2025. [Online]. Available: https://github.com/NilsBade/AntRig-Measurement-System.git

[22] Rat Rig, Lda. *RatRig V-Core* 3.1. Accessed: Jul. 28, 2025. [Online]. Available: https://docs.ratrig.com/product-details/v-core3-1

[23] *Klipper Website*. Accessed: Aug. 2, 2025. [Online]. Available: https://www.klipper3d.org/

[24] *Octoprint Website*. Accessed: Aug. 2, 2025. [Online]. Available: https://octoprint.org/

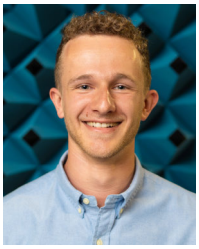
[25] ITEM KH. *ITEM Industrietechnik GmbH*. Accessed: Jul. 28, 2025. [Online]. Available: https://www.item24.com/en-de/profile-kh-8-40x40-anthracite-64161

[26] W. L. Gore & Associates, Inc. *General Purpose Test and Interconnect Applications*. Accessed: Nov. 18, 2025. [Online]. Available: https://www.gore.com/products/microwave-RF-assemblies-general-purpose

[27] A. C. Newell, "Error analysis techniques for planar near-field measurements," *IEEE Trans. Antennas Propag.*, vol. 36, no. 6, pp. 754–768, Jun. 1988.

[28] U. Stumper, "Influence of nonideal calibration items on S-parameter uncertainties applying the SOLR calibration method," *IEEE Trans. Instrum. Meas.*, vol. 58, no. 4, pp. 1158–1163, Apr. 2009.

[29] B. Tegowski, D. Langer, N. C. Albrecht, and A. Koelpin, "Analysis of the radar channel and its variability in vital-sign sensing applications," *IEEE Trans. Antennas Propag.*, vol. 74, no. 2, pp. 1980–1992, Feb. 2026.



NILS BADE received the B.Sc. and M.Sc. degrees in mechatronics from Hamburg University of Technology, Hamburg, Germany, in 2021 and 2025, respectively, where he is currently pursuing the Ph.D. degree with the Institute of High-Frequency Technology.

His research interests include wireless synchronization techniques, next-generation mobile communication systems, and development of measurement systems for high-frequency applications.



DOMINIK LANGER (Graduate Student Member, IEEE) received the B.Sc. and M.Sc. degrees in electrical engineering from Hamburg University of Technology, Hamburg, Germany, in 2018 and 2021, respectively, where he is currently pursuing the Ph.D. degree with the Institute of High-Frequency Technology.

His current research interests include antenna design, additive manufacturing, and interferometric radar systems.

Mr. Langer was a recipient of the First Prize of the Radar for Noncontact Vital Sign Sensing of IEEE International Microwave Symposium in 2021, 2022, and 2023, respectively. He serves as a reviewer for *IEEE Microwave and Wireless Technology Letters*.



ALEXANDER KOELPIN (Fellow, IEEE) received the Diploma degree in electrical engineering and the Ph.D. and habilitation degrees from the University of Erlangen-Nuremberg (FAU), Erlangen, Germany, in 2005, 2010, and 2014, respectively.

From 2005 to May 2017, he was with the Institute for Electronics Engineering, FAU. From 2007 to 2010, he was a Team Leader; from 2010 to 2015, a Group Leader of circuits, systems, and hardware test; and since 2015, he has been a Leader of the Group Electronic Systems. From June 2017 to February 2020, he was a Professor and the Head of the Chair for Electronics and Sensor Systems, Brandenburg University of Technology Cottbus-Senftenberg, Cottbus, Germany. Since March 2020, he has been with Hamburg University of Technology, Hamburg, Germany, as a Professor and the Head of the Institute of High-Frequency Technology. He has authored or co-authored more than 300 publications in his areas of interest. His research interests are in the areas of microwave circuits and systems, radar and wireless sensing, wireless communication systems, local positioning, and six-port technology.

Dr. Koelpin was a member of the Commission A: Electromagnetic Metrology of U.R.S.I. He has been an Elected Member since 2018. He was awarded the IEEE MTT-S Outstanding Young Engineer Award in 2016, the ITG Award of the German VDE in 2017, and the IEEE Microwave Application Award in 2026. Furthermore, he serves as a reviewer for several journals and conferences. He was the Chair of the IEEE MTT-S Technical Committee MTT-24 from 2018 to 2020, and has been the Vice Chair of the IEEE MTT-S/AP German Chapter Executive Board since 2020. He served as the Conference Chair for the 2020 German Microwave Conference, the Technical Program Chair for IEEE Radio and Wireless Week 2021, and the General Chair for IEEE Radio and Wireless Week 2023.